Activation of the cGAS-STING innate immune response in cells with deficient mitochondrial topoisomerase TOP1MT

Iman Al Khatib(1), Jingti Deng(1), Symes Andrew Symes(2), Hongliang Zhang(3), Sharyin Huang(3), Yves Pommier(3), Aneal Khan(4,5), William Gibson(6), Timothy E Shutt(7)*

1) Department of Biochemistry & Molecular Biology, Cumming School of Medicine, University of Calgary; Alberta Children's Hospital Research Institute; Calgary, Alberta, Canada, T2N 4N1.
2) Department of Geomatics Engineering, Schulich School of Engineering, University of Calgary, Calgary, Alberta, Canada T2N 1N4.
3) Laboratory of Molecular Pharmacology, Developmental Therapeutics Branch, Center for Cancer Research, NCI, National Institutes of Health, Bethesda, MD, 20892, USA.
4) Discovery DNA, Calgary, Alberta, T2L 1Y8, Canada
5) M.A.G.I.C. Clinic Ltd. (Metabolics and Genetics in Calgary); Department of Pediatrics, Cumming School of Medicine, University of Calgary; Alberta Children's Hospital Research Institute; Calgary, Alberta, Canada, T2M OL6.
6) Department of Medical Genetics, Faculty of Medicine, University of British Columbia; British Columbia Children's Hospital Research Institute Vancouver; British Columbia, Canada, V5Z 4H4.
7) Departments of Medical Genetics and Biochemistry & Molecular Biology, Cumming School of Medicine, University of Calgary; Alberta Children's Hospital Research Institute; Hotchkiss Brain Institute; Calgary, Alberta, Canada. T2N 4N1.

*Corresponding Author: timothy.shutt@ucalgary.ca

Abstract

Systemic lupus erythematosus (SLE) is an autoimmune condition where the underlying dysfunction is often unknown. Here, we identify a novel link between the mitochondrial topoisomerase TOP1MT and SLE, as a novel variant predicted to affect TOP1MT function, P193L, was identified in a family with SLE and other autoimmune diseases. Although there was no previous genetic association between *TOP1MT* and SLE, the role of TOP1MT as a regulator of mtDNA led us to investigate whether TOP1MT could mediate the release of mtDNA to the cytosol, where it could then activate the cGAS-STING innate immune pathway. This pathway increases the expression of type-I interferons and is known to be activated in some patients with SLE. Through analysis of cells lacking TOP1MT, or re-expressing the P193L variant, we established a new association by which TOP1MT dysfunction leads to increased release of mtDNA to the cytosol, causing activation of the cGAS-STING pathway. We also characterized the P193L variant for its ability to rescue several TOP1MT functions in *TOP1MT* knockout cells. While re-expression of the P193L variant was able to rescue steady state mtDNA copy number, most functions investigated only showed partial rescue, including repletion of mtDNA replication following depletion, nucleoid size, steady state mtDNA transcripts levels, and mitochondrial morphology. Meanwhile, the P193L variant failed to rescue decreased mitochondrial respiration. Overall, these findings support the notion that P193L variant is not fully functional and likely influences susceptibility to SLE via cGAS-STING mediated activation of the innate immune system.

Introduction

The innate immune response is the first line of defense against various microorganisms and pathogens. However, the immune system sometimes recognizes intracellular components as foreign and attacks its own tissue and organs, leading to autoimmune diseases. The exact cause for such erroneous autoimmune responses is not always understood, as there are many triggers that can lead to the self-reactivity of the immune system. Systemic lupus erythematosus (SLE) is a chronic, heterogenous, systemic autoimmune disease, in which accumulating evidence suggests that mitochondrial dysfunction plays important role[1, 2]. Multiple genetic variants including monogenic variants have been associated with lupus susceptibility, which provides significant insight into the cause, mechanisms, and potential treatment options for patients[3-6].

Mitochondria, best known as the powerhouses of the cell, are eukaryotic organelles that evolved from aerobic prokaryotes through an endosymbiotic event that occurred billions of years ago[7]. The strongest evidence for their bacterial origin is the fact that mitochondria have retained their own 16,569 bp circular genome, known as mitochondrial DNA (mtDNA), which is present in hundreds to thousands of copies in the cell[8]. Release of mtDNA into the cytosol, in response to pathogen-induced mitochondrial stress, is a mechanism by which cells can amplify innate immune signaling in response to pathogen invasion[9, 10]. However, in the absence of pathogens, mitochondrial dysfunction can also cause release of mtDNA into the cytosol, leading to 'sterile' activation of the innate immune system[11-13]. The mechanism of release of mtDNA into the cytosol has been studied primarily in the context of apoptosis, where it depends on the opening of mitochondrial permeability transition (MPT) pores in the inner mitochondrial membrane[14], and oligomerization of voltage-dependent anion channel (VDAC) in the mitochondrial outer membrane[15]. While less is known about when and how mtDNA is released under more physiological conditions, there is a growing appreciation of the functional consequences with respect to inflammation and disease. Recent research has demonstrated that release of mtDNA into the cytosol can activate innate immune pathways mediated by Toll-like receptor 9 (TLR9), Nod-like receptor NLRP3 inflammasome, and of particular relevance here, the cGAS-STING pathway[16].

The cGAS-STING pathway is an immune response that recognizes cytosolic dsDNA, which can come from a variety of sources including the mitochondria[17-19]. Upon binding to dsDNA, cGAS (cyclic GMP-AMP synthase) dimerizes and becomes activated, whereupon it

catalyzes the synthesis of cyclic dinucleotide cGAMP (2′3′ cyclic GMP–AMP) from ATP and GTP. These cGAMP dinucleotides then bind STING (stimulator of interferon genes), causing conformational changes that lead to STING oligomerization and subsequent translocation from the endoplasmic reticulum (ER) to the Golgi apparatus[20, 21]. This activated STING recruits TANK-binding kinase 1 (TBK1)[16], which causes a series of events leading to phosphorylation of interferon regulatory factor 3 (IRF3). In turn, the phosphorylated IRF3 translocates to the nucleus where it induces expression of type I interferons, interferon-stimulated genes (ISGs), and several other inflammatory mediators, pro-apoptotic genes, and chemokines[20].

The first work linking mtDNA to the cGAS-STING pathway showed that depletion of the mitochondrial DNA packaging protein TFAM led to cytosolic release of mtDNA, resulting in cGAS-STING activation[22]. More recently, deficiency in the mitochondrial CLPP (Caseinolytic mitochondrial matrix peptidase proteolytic subunit) protease subunit was also shown to result in mtDNA instability and activation of type I IFN signaling through cGAS-STING[23]. Meanwhile, cytosolic mtDNA release[24] and activation of cGAS-STING have also been implicated in Parkinson disease[25]. Many inflammatory diseases also show activation of cGAS-STING in damaged organs, like liver [26-28], kidney [29, 30] and pancreas[31]. The involvement of TFAM and CLPP in mtDNA release into the cytosol and cGAS-STING activation raises the question of whether impairment of mtDNA maintenance caused by coding variants in other proteins might have similar consequences. One intriguing candidate is TOP1MT, a topoisomerase that helps resolve crossovers and knots that can originate during maintenance of the circular mtDNA genome. TOP1MT is the only human topoisomerase that is solely present in the mitochondria[32-34], where it plays important roles in mtDNA replication, transcription, and translation[35-38]. Interestingly, a wide range of autoantibodies have been described and detected in the serum of SLE patients[39, 40] including anti-double-stranded DNA (anti-dsDNA)[41, 42] and autoantibodies recognizing the nuclear topoisomerase enzyme TOP1[43-46] as well as the mitochondrial TOP1MT[47].

Here, we characterize a Variant of Unknown Significance in TOP1MT, P193L, identified in a family with several members who presented with SLE and a variety of other autoimmune disorders. Notably, activation of the cGAS-STING pathway has been linked to SLE[48, 49]. For example, an activating mutation in STING causes lupus-like manifestations[50]. To date, the connection between cGAS-STING activation in SLE has been noted in the context of nuclear

DNA present in the cytosol[49, 51]. Meanwhile, inhibition of VDAC-mediated cytosolic mtDNA release was beneficial in a mouse model of SLE[15], suggesting a role for cytosolic mtDNA in promoting SLE. Here, we uncover a novel connection between TOP1MT dysfunction and activation of the cGAS-STING pathway, which may partially explain the autoimmune phenotype in several members of this family, and provide further evidence for the role of mtDNA in the pathogenesis of SLE.

Materials and Methods

Mutation identification

In accordance with the principles of the Declaration of Helsinki, all study participants provided informed consent to next-generation sequencing as part of the BCCHRI study "Comprehensive Characterization of Genetic Disorders of Body Weight" (UBC CREB Study approval number H08-00784).

Cell culture

McCoy's 5A (modified) media (Gibco, 16600-82) containing l-Glutamine and supplemented with 10% fetal bovine serum (FBS) was used to culture HCT 116 control (HCT WT), HCT 116 TOP1MT-KO (HCT KO) and stably transfected cells. Cells were seeded at 1.5 x 10^6 cells seeding density in 10cm plates and allowed to grow for two days before being harvested for analysis. DMEM (Gibco, 11965092) supplemented with 10% FBS was used for Phoenix cells for the retrovirus generation. All cells were maintained at 37 °C and 5% CO_2.

Plasmids & cloning

The retroviral vector pRV100G backbone was used to insert TOP1MT open reading frame (ORF) followed by C-terminal T2A mCherry tag. Site directed mutagenesis was used to introduce the C578T variant in TOP1MT. The empty vector control was missing the TOP1MT ORF and only contained the backbone with T2A mCherry.

Generation of stable lines

Stable cells expressing wild type TOP1MT (NM_052963.2), TOP1MT P193L variant, or empty vector controls were generated via retroviral transduction. Briefly, Phoenix cells were

transfected with the retroviral plasmids. Then the HCT WT or HCT KO cells were transduced using 5 ml of the supernatant containing virus after 48 and 72 hrs in 100 mm plates. Following transduction, Flow cytometry sorting was done for the red fluorescence from approximately $6X10^6$ cells were using a 130 μm nozzle on a BD FACSAria Fusion (FACSAriaIII) cytometer (BD Biosciences), supported by FACSDiva Version 8.0.1. As for the cells with low expression of TOP1MT, all the positively expressing red fluorescent cells were subjected to sorting again separating them into low threshold, intermediate and high expression red fluorescence gates.

PCR and sequencing

PureLink Genomic DNA Mini Kit (Thermo Fisher Scientific, K182001) was used for total DNA extraction. TOP1MT cDNA was amplified by PCR using the forward primer CACAACAAAGGAGGTTTTCCGGAAG and the reverse primer TGCAGTCCTTCCCCAGGA to confirm the success of the transduction. The amplified band was further purified and sequenced using Sanger sequencing to confirm the variant status of TOP1MT.

Live cell imaging

Live cell imaging was done on 35 mm glass bottom dishes, 8×10^4 cells were seeded and grown for two days. MitoTracker Red (50 nM) (Thermo Fisher Scientific, M7512) and PicoGreen (Thermo Fisher Scientific, P7581) (3 μL/mL) were used to visualize mitochondrial networks and mtDNA nucleoids respectively[38, 52].

Immunofluorescence staining

1.5×10^4 cells were seeded over 12 mm glass coverslips (no. 1.5) in 24 wells plates and incubated for 2 days. Subsequently, cells were fixed with 4% paraformaldehyde and stained with mitochondrial networks labeled with a primary antibody against TOMM20 (Sigma-Aldrich, HPA011562) used at 1:1000, STING (D2P2F) (Cell signaling, 13647S) used at 1:300, endoplasmic reticulum ER Calnexin (Millipore Sigma, MAB3126) at 1:1000 and Golgi TGN46 (Proteintech, 66477-1-Ig) used at 1:500. The corresponding Alexa fluor-conjugated secondary antibodies (Thermo Fisher Scientific) were used at 1:1000.

Microscopy

An Olympus spinning disc confocal system (Olympus SD OSR) (UAPON 100XOTIRF/1.49 oil objective) was used to image fixed samples and the microscope was operated by Metamorph software. Whenever there was live imaging, a cellVivo incubation module was used to maintain cells at 37 °C and 5% CO_2.

Image analysis for mtDNA nucleoids

The particle analysis tool in ImageJ FIJI was used to measure nucleoid size after binarizing the images[53]. A region of interest in cells stained with PicoGreen was manually selected including all the mitochondrial network of the cell but excluding the nucleus, then the surface area of each nucleoid was automatically determined using the analyze particles feature. The nucleoids from at least 10 cells were measured. Data was represented by a violin plot representing the distribution of the average mtDNA nucleoid sizes per cell for the indicated cell lines. P values were based on unpaired, 2-tailed Student's t-tests.

Image analysis for mitochondrial networks

Images of the cells stained with anti-Tomm20 (Sigma-Aldrich, HPA011562) were used for qualitative evaluation of the mitochondrial network morphology. The network was classified into three categories, fragmented (predominantly small mitochondrial fragments), intermediate (cells containing a mixture of short fragments and elongated networks) and fused (elongated, interconnected networks with few to no short fragments)[52]. At least 50 cells from three independent biological replicates were scored for each of the investigated cell lines. The results shown represent means ± SEM, and P values were based on unpaired, 2-tailed Student's t-tests.

Image analysis for STING localization

Images of the cells stained with anti-STING (D2P2F) (Cell signaling, 13647S), anti-Calnexin (Millipore Sigma, MAB3126) and anti-TGN46 (Proteintech, 66477-1-Ig) were used for quantitative evaluation of the localization of STING to either the ER or the Golgi. Images were binarized, then the surface area of the total STING signal or the localized signal to the corresponding organelle were measured. The ratio of the localized area to the total STING area was determined from at least 10 images. Data was represented as means ± SEM, and P values were based on unpaired, 2-tailed Student's t-tests.

mtDNA copy number analysis

The PureLink Genomic DNA Mini Kit (Thermo Fisher Scientific, K182001) was used to isolate total DNA from cultured cells using according to the manufacturer's protocol. Quantitative PCR (QPCR) was used to determine mtDNA copy number [54]. Primers shown in Table 1 for mtDNA or 18S DNA were used with PowerUp SYBR Green Master Mix (Thermo Fisher Scientific, A25742) to amplify 50-100 ng of DNA template, in the QuantStudio 6 Flex Real-Time PCR system (Thermo Fisher Scientific) machine. The delta delta Ct method was used to determine mtDNA copy number using the 18S gene as a reference. Reactions were performed in three technical replicates and mtDNA copy number analysis was performed on at least three independent biological replicates. Data is presented as mean ± SEM and unpaired, 2-tailed Student's t-tests were used to determine statistical significance.

Ethidium bromide depletion/repletion

1μg/ml Ethidium bromide (Fisher Scientific, 15-585-011) was used to deplete the cells from their mtDNA content for three days, as described previously[55], then fresh media was added afterwards to allow the cells to recover their mtDNA copy number. Cell pellets from the days 0, 3, 6 and 8 were collected for DNA purification and copy number analysis.

Western blot

RIPA buffer (Thermo Scientific™, 89900) containing protease inhibitors was used to lyse collected cell pellets after washing with 1× phosphate buffered saline (PBS). SDS-PAGE gels were used to resolve 50 μg of total cell lysates from different cell lines then PVDF membranes were used for the transferred blot. Blots were probed with several antibodies at the indicated dilutions; OxPhos antibody cocktail (Abcam, ab110411; 1:500 dilution), anti-Actin (Sigma, A5316; 1:1000), anti-MTCO2 (Abcam, ab110258; 1:1000), anti-GAPDH (Millipore Sigma, ABS16; 1:1000), anti-TOP1MT-3 (Developmental Studies Hybridoma Bank, CPTC-TOP1MT-3; 1:200). Appropriate horseradish peroxidase (HRP)-conjugated secondary antibodies were used at 1:3000 as follows: goat anti rabbit IgG, HRP linked Antibody (Cell Signaling Technology, 7074S), or goat anti-mouse IgG-HRP (Santa Cruz Biotechnology, sc-2055). The

Clarity ECL substrate (Biorad, 1705061) was used to expose the horseradish enzyme attached to each antibody using an Amersham Imager AI600.

Southwestern blot

Cells were treated with 10 uM Aphidicolin (HelloBio Ltd, Bristol UK) for 4 hours to inhibit nuclear DNA synthesis, then 50 uM BrdU (Invitrogen, fisher scientific) is added for another 24 hours. Total DNA was isolated from $2X10^7$ cells according to the instruction of E.Z.N.A Tissue DNA kit. As controls, 1ug of DNA was treated with 10U of Topoisomerase I (New England Biolabs) at 37°C for 1 hour, or BamHI 20 U (New England Biolabs) at 37°C for 1 hour. DNA samples (1ug) were then separated on a 0.45% agarose gel (Biotechnology VWR, life science) at 30V 18-20 hours in cold room. The gel was washed briefly with water and soaked in denaturing buffer (0.5N NaOH, 1.5M NaCl) for 45-60 mins. The gel was washed again in water and soaked in 10X saline-sodium citrate (SSC) for 30 mins. Transfer to PVDF membrane (Bio-Rad, Cat# 1620177) was done using capillary action as described previously (Nature protocols, 518, 2006). The PVDF membrane was washed in 6X SSC for two minutes, and the DNA bands on the membrane were immobilized by UV-crosslinking (UV Stratalinker 1800). After blocking with 10% non-fat dry milk for 1h, the PVDF membrane was incubated for 2 h at 20 ˚C with anti-BrdU antibody (1:2000X dilution in TBST, Becton Dickinson Immunocytometry Systems), followed by incubations with corresponding horseradish peroxidase (HRP)-conjugated goat polyclonal anti-mouse IgG (1:5,000 dilution, EMD Millipore Etobicoke, Ontario, Canada). Blots were developed with Supersignal West Femto enhanced chemiluminescence substrate (Thermo Scientific) and imaged using the chemiluminescence imaging analyzer (LAS3000mini; Fujifilm, Tokyo, Japan).

RNA extraction and quantification

The E.Z.N.A.® HP Total RNA Kit, Omega Bio-tek® (VWR Scientific, CA101414-850) was used for RNA extraction from cell pellets according to the manufacturer's protocol. Following extraction, 7.5 µg of RNA was reverse transcribed by iScript™ Advanced cDNA Synthesis Kit (Biorad, 1725038) to generate cDNA. Quantitative PCR with PowerUp SYBR Green Master Mix (Thermo Fisher Scientific, A25742) was used to amplify the genes of interest according to the primers mentioned in the Table 1 from 15-20 ng of cDNA in the QuantStudio 6

Flex Real-Time PCR system (Thermo Fisher Scientific) machine. Actin expression was used as the control in the delta delta Ct method to determine the relative expression of various transcripts. Reactions were performed in triplicate and mtDNA copy number analysis was performed on at least three independent biological replicates. Data is presented as mean ± SEM and unpaired, 2-tailed Student's t-tests were used to determine statistical significance.

Gene	Forward Primer	Reverse Primer
18 S	TAGAGGGACAAGTGGCGTTC	CGCTGAGCCAGTCAGTGT
mito	CACCCAAGAACAGGGTTTGT	TGGCCATGGGTATGTTGTTAA
COX I	GACGTAGACACACGAGCATATTTCA	AGGACATAGTGGAAGTGAGCTACAAC
ND 6	CAAACAATGTTCAACCAGTAACCACTAC	ATATACTACAGCGATGGCTATTGAGGA
Cyt B	ATCACTCGAGACGTAAATTATGGCT	TGAACTAGGTCTGTCCCAATGTATG
Actin	AAGACCTGTACGCCAACACA	AGTACTTGCGCTCAGGAGGA
INF-α	AAATACAGCCCTTGTGCCTGG	GGTGAGCTGGCATACGAATCA
INF-β	AAGGCCAAGGAGTACAGTC	ATCTTCAGTTTCGGAGGTAA
INF-γ	CGCCTTGGAAGAGTCACTCA	GAAGCCTCAGGTCCCAATTC
STING	GAGCAGGCCAAACTCTTCTG	TGCCCACAGTAACCTCTTCC
D-loop 1	TTTCCCCTCCCACTCCCATA	GTGTGTGTGCTGGGTAGGAT
D-loop 2	CACCCAAGAACAGGGTTTGT	TGGCCATGGGTATGTTGTTAA

Table 1: Primers used for quantitative PCR for detection of indicated genes.

Cytosolic mtDNA quantification

Cell pellet was resuspended in roughly 500 µl buffer containing 150 mM NaCl, 50 mM HEPES, pH 7.4, and 15–25 µg/ml digitonin (Sigma Aldrich, D141). The homogenates were incubated end over end for 25 minutes to allow selective plasma membrane permeabilization, then centrifuged at 980 g for 10 min to pellet intact cells. The first pellet was used to extract total DNA using the PureLink Genomic DNA Mini Kit (Thermo Fisher Scientific, K182001). The cytosolic supernatants were transferred to fresh tubes and spun at 17000 g for 10 min to pellet any remaining cellular debris, yielding cytosolic preps free of nuclear, mitochondrial, and ER contamination. DNA was then isolated from these pure cytosolic fractions using the PureLink Genomic DNA Mini Kit (Thermo Fisher Scientific, K182001). qPCR was performed on both whole cell extracts and cytosolic fractions using nuclear DNA primers (18S) and mtDNA

primers (D loop1-2, CytB, COX I, ND 6) as indicated in Table 1, and the CT values obtained for mtDNA abundance for whole cell extracts served as normalization controls for the mtDNA values obtained from the cytosolic fractions. This allowed effective standardization among samples and controlled for any variations in the total amount of mtDNA in control and stable cell lines samples.

cGAS inhibition and recovery

RU.521 (Invivogen, inh-ru521) was used at a concentration of 5 ug/ml to inhibit cGAS in cells seeded in 10 cm plates, after 24 hours fresh media was added to the cells to recover for another 24 hours. Similar volume of DMSO was used as a negative control to eliminate any effect of the drug solvent.

Structural modeling

Structural models for the TOP1MT variants were generated via RoseTTAFold, a deep learning solution to predicting protein structures, which was conducted on the Robetta web server[56]. Five structures were generated per mutant, the structure with the highest confidence level was selected for further use in analysis. Once the structures were selected for each mutant, HADDOCK was used to perform docking[57, 58]. The binding strength and location of the binding were approximated to generate models with both short (10) and long (50) strands of mtDNA, with sequences detailed in the following reference[35, 59]. Short strand docking offered insight into the highly charged barrel through the middle of the protein. Long strand modelling then mixed the barrel analysis with the stabilizing forces of the surrounding protein structure. The most probable binding sites were identified and fit by HADDOCK and the model selected was the one with the best HADDOCK score. These models and the interaction lists generated around them were used then to compare the binding efficacy and form between the mutants and the wild type. Models were downloaded, screened and visualized in Pymol[60].

Results

The family was originally ascertained on the basis of congenital leptin deficiency in the index patient's daughter[61]. However, the proband for the lupus phenotype is A1020 (the mother). She has been diagnosed with hypothyroidism, systemic lupus erythematosus, Sjogren's syndrome, fibromyalgia with peripheral neuropathy. Now in her mid 50s, she has moderate to severe pulmonary fibrosis. She is thought to have celiac disease as well, though the latter is not biopsy-proven.

Variant Identification

Chromosomal microarray studies did not identify any microdeletions or microduplications that met clinical criteria for being considered pathogenic or likely pathogenic. Exome sequencing in members of the proband's nuclear family did not identify any known pathogenic variants in recognized Mendelian disorders. However, TOP1MT was flagged as a potential genetic cause of monogenic systemic lupus erythematosus (SLE) when a P193L missense variant was discovered in the consanguineous family, with multiple members affected by pediatric-onset autoimmune disease, including SLE (Fig 1a). The P193L variant is a result of a point mutation at cDNA position 578C>T (NM_052963.2) that results in a proline to leucine change at amino acid 193, which predicted to be possibly damaging and deleterious with minor allele frequency (MAF) of 0.00002786 in Genome Aggregation Database (GnomAD v3.1.2). The identified variant occurs at a highly conserved site in the core domain of TOP1MT (Fig 1b), which is located within the DNA binding barel (Fig 1c).

Preliminary functional studies in patient-derived white blood cells found that family members that were either heterozygous (TOP1MT $^{mut/+}$) or homozygous (TOP1MT $^{mut/mut}$) for the P193L variant showed impaired oxidative phosphorylation (OXPHOS) and increased ROS, indicative of mitochondrial dysfunction (Gibson lab, unpublished data). However, additional work was necessary to confirm whether the P193L variant impacts the functionality of TOP1MT, and to investigate potential mechanisms that might link TOP1MT to SLE.

Activation of cGAS-STING signaling in *TOP1MT* HCT KO cells

Given the SLE and other autoimmune disease phenotypes in the family, and the role of TOP1MT as a mediator of mtDNA, we hypothesized that TOP1MT dysfunction could contribute

to cytosolic release of mtDNA and activation of the cGAS-STING pathway. To investigate this notion, we took advantage of HCT116 cells wherein TOP1MT had been knocked out via CRISPR-Cas9[55]. We first measured the abundance of mtDNA present in cytosol extracts. Using several primer sets that amplify distinct regions of the mtDNA, quantitative PCR consistently detected significantly higher levels of mtDNA in the cytosol extracts of HCT116 *TOP1MT* KO cells (HCT KO) compared to HCT116 wild type (HCT WT) (Fig 2a). Next, we wanted to see if the increased cytosolic mtDNA leads to increased expression of type I interferons. Consistent with activation of the cGAS-STING signaling pathway, both interferon-alpha (INF-α) and interferon- beta (INF-β) were elevated in HCT KO cells. However, levels of the type II interferon-gamma (INF-γ), which is not regulated by cGAS-STING was not altered (Fig 2b). As there are multiple activators of innate immune responses, we wanted to confirm that this type I interferon elevation occurred through the cGAS-STING pathway. To this end, 24 hr treatment of cells with RU.521, an inhibitor of cGAS[62], led to lower interferon levels among HCT KO cells, whereas basal levels in HCT WT cells remained unchanged (Fig 2c & 2d). Subsequently, upon removal of RU.521, the interferon levels were further elevated again in HCT KO cells relative to HCT WT controls (Fig 2e). Collectively, these novel findings show that loss of TOP1MT results in increased levels of cytosolic mtDNA, and increased cGAS-STING dependent expression of the INF-α and INF-β.

Generation of Cell line

Given the mitochondrial dysfunction noted in patient derived blood cells, we wanted to examine the ability of TOP1MT's P193L variant to rescue multiple mitochondrial parameters known to be impaired in HCT KO cells[38]. As described previously[38], starting from HCT WT and HCT KO, we generated four different stable cell lines using retroviral constructs expressing TOP1MT and the mCherry fluorescent protein separated by a self-cleavage peptide (TOP1MT-T2A-mCherry), or an empty vector control. This construct leads to expression of TOP1MT, which will be directed to the mitochondria by the mitochondrial targeting sequence, and mCherry, which can be used to monitor transduction. Two control cell lines, henceforth referred to as WT-ctrl and KO-ctrl, were generated by transducing an empty vector expressing only mCherry in the HCT WT and HCT KO cells respectively. A third cell line was generated by

re-expressing wild type TOP1MT (indicated as Rescue). Finally, a fourth cell line expressing the patient variant P193L was also established (referred to as P193L).

Expression of mCherry was used to sort the positively transduced cells by flow cytometry. Transduction was further confirmed by PCR amplification of the inserted TOP1MT open reading frame (Fig 3a), and DNA sequencing to confirm the identity of the Rescue and the P193L variant cell lines (Fig 3b). Next, immunoblotting was used to confirm the expression of TOP1MT proteins (Fig 3c). A band of the predicted size of ~70 kDa corresponding to TOP1MT protein was observed WT-ctrl, Rescue and P193L cells, but not in the KO-ctrl cells (Fig 3d). Notably, the levels of TOP1MT protein in the Rescue and P193L lines was ~10-fold higher than the endogenous TOP1MT protein levels in the WT-ctrl cells. Further validation of the protein expression was confirmed via immunofluorescence imaging, where overexpressed TOP1MT protein was detected, and confirmed to localize to mitochondria (Fig 3e).

Next, we wanted to determine the ability of the P193L variant to rescue the aberrant functions previously identified in HCT KO cells[38], including: reduced nucleoid size, the hyperfused mitochondrial network, and decreases in mitochondrial transcription, mtDNA replication, mitochondrial translation and oxidative phosphorylation.

Nucleoids

Based on our previous work[38], and the role of TOP1MT in preventing negative supercoiling of mtDNA[63]. To look at supercoiling, we used a southwestern blot approach that labels mtDNA with Brdu, which can then be separated on an agarose gel, transferred to a membrane and visualized by immunoblotting. To confirm which bands represent linear, relaxed, or supercoiled mtDNA, DNA was treated with either BamHI or Topoisomerase enzymes. Consistent with the expected reduction of topoisomerase activity, we found that KO-ctrl cells had a higher ratio of supercoiled to relaxed mtDNA compared to WT-ctrl cells, and that this was reversed in the Rescue cells (Fig 4a). Though the P193L line appeared to show increased supercoiling mtDNA relative to the rescue line, the ratio of supercoiled mtDNA to the relaxed mtDNA was not significantly altered (Fig 4b).

As an alternative approach to gain insight on the mtDNA topology, we quantified the size of individual nucleoids stained with PicoGreen using confocal microscopy (Fig 4c). As expected, and consistent with the southwestern blot analysis showing increased supercoiling, mtDNA

nucleoids were significantly smaller in KO-ctrl cells, and this was reversed by overexpression of the WT TOP1MT in the Rescue line. However, the overexpression of the P193L variant failed to fully rescue the nucleoid sizes (Fig 4d) to the same level as the WT protein, suggesting that this variant has reduced topoisomerase activity.

Mitochondrial Morphology

The mitochondrial network is dynamic and can change in response to various physiological cues. In KO-ctrl cells, mitochondrial networks imaged by confocal microscopy were more fused than their WT-ctrl counterparts, and this was reversed by re-expression of the WT protein in the Rescue cells (Fig S1a). However, expression of the patient variant had an intermediate effect on mitochondrial morphology (Fig S1b), consistent with the variant being unable to completely rescue the effects of TOP1MT loss.

Mitochondrial Transcription

We next examined the expression of mtDNA-encoded transcripts, as the supercoiling extent of mtDNA directly influences the transcription of the mitochondrial genome[36-38]. While the WT TOP1MT could restore mitochondrial transcript levels, the P193L variant was slightly less efficient at doing so (Fig 5a). This reduced rescue is likely because TOP1MT alters mtDNA topology, which impacts mitochondrial transcription *in vitro*[64-68].

mtDNA copy number and replication

In addition to the effect of transcription, we wanted to determine the ability of the P193L variant to restore the elevated mtDNA copy number (Fig 5b) and reduced mtDNA replication rates (Fig 5c) observed in KO-ctrl cells. In this regard, the P193L variant was able to rescue steady-state mtDNA copy number levels to a similar degree as the WT protein. To look at mtDNA replication rates, we monitored the rescue of mtDNA copy number following depletion by ethidium bromide. While the P193L variant showed improved mtDNA repletion compared to the HCT KO cells, with nearly complete rescue by day 8, mtDNA replication was significantly slower than that in cells re-expressing the WT TOP1MT protein, again indicative of reduced functionality.

Expression of Mitochondrial Proteins

As TOP1MT can also impact the translation of mitochondrial proteins independently of its topoisomerase activity and changes in transcripts[38], we studied the effect of P193L on the expression of oxidative phosphorylation (OxPhos) proteins encoded by both the nucleus (NDUFB8, SDHB, UQCRC2 and ATP5) and mtDNA (COXII) (Fig 5d). Notably, global OxPhos protein levels can reflect mitochondrial translation, as the levels of nuclear-encoded OxPhos proteins depends on the expression of mtDNA encoded subunits[69]. Expression of Complex I subunits NDUFB8, Complex II subunit SDHB, Complex III subunit UQCRC2, Complex IV subunit COXII and Complex V subunit ATP5A (Fig 5e) showed similar trends with reduced expression in P193L cells compared to Rescue. Although we did not see a significant decrease in SDHB and UQCRC2 in these experiments, the results were trending in the same direction. Combined, these results indicate that the P193L variant is unable to completely restore reduced OxPhos proteins expression.

Mitochondrial Respiration

Following up on the changes in OxPhos proteins, we next investigated mitochondrial respiration in our stable cell lines (Fig 5f) to examine if the reduced expression of OxPhos proteins affect the oxygen consumption and mitochondrial energy production. As seen previously[38, 70], we found that basal respiration (Fig 5g), maximal respiration (Fig 5h), and ATP-coupled respiration (Fig 5i), were all reduced in the KO-ctrl cells, and restored by re-expressing the WT TOP1MT protein. However, the Rescue cells expressing P193L patient variant showed no rescue at all relative to the KO-ctrl cells.

cGAS STING pathway in rescue cell lines

Finally, we wanted to examine the effect of the P193L variant on the novel cGAS-STING pathway activation that we described above in the HCT KO cells. For this purpose, we started by looking at the cytosolic mtDNA levels. Unexpectedly, both lines stably overexpressing either WT or P193L forms of TOP1MT rescued the cytosolic mtDNA levels to the same extent (Fig 6a). Similarly, qRT-PCR analysis of type I interferon expression was rescued in HCT KO cells overexpressing either WT or P193L forms of TOP1MT (Fig 6b). However, it must be noted

again that both lines express TOP1MT protein at approximately 10-fold above endogenous levels, which could be compensating for a loss of activity in the P193L protein.

Characterization of low re-expression of P193L and WT TOP1MT variants

To avoid the complications of high level TOP1MT protein expression, we used flow cytometry to sort for cells expressing relatively low levels of mCherry, which should correlate directly to TOP1MT protein expression. As shown by western blot (Fig 6c), we were able to select a population of cells expressing TOP1MT protein much closer to endogenous levels (Fig 6d). These lines were labeled Rescue low, and P193L low. Next, we analyzed the cytosolic mtDNA levels from these cells. While the low-level expression of TOP1MT WT was still able to rescue the cytosolic mtDNA levels, the low-level expression of the P193L variant was unable to provide rescue (Fig 6e). In a similar fashion, the type I interferon levels remained elevated in cells expressing low levels of the P193L variant, but were restored to normal in cells expression low level of the WT form (Fig 6f). However, low-level expression of other TOP1MT variants linked to cardiomyopathy (Fig S2 a&b), namely R198C and V338L, fully rescued the cytosolic mtDNA (Fig S2c) and the interferon levels (Fig S2d), suggesting that the elevated cGAS-STING is specific to the P193L variant and pathogenic autoimmune activation.

Previous reports have indicated the translocation of activated STING from the ER to the Golgi[71]. Thus, as another means to examine activation of the cGAS-STING pathway, we used immunofluorescence to monitor the cellular localization of STING. Notably, there is a stronger co-localization signal between STING and the ER in both WT-ctrl and Rescue lines, compared to the KO-ctrl and P193L low lines (Fig 7a&b). Conversely, there was higher levels of colocalization between STING and Golgi in the KO-ctrl and P193L low cells, compared to WT-ctrl and Rescue cell line (Fig 7c&d). Altogether, these data provide support for the notion that the P193L variant leads to activation of the cGAS-STING innate immune pathway via promoting the cytosolic release of mtDNA.

Discussion

The discovery of the novel TOP1MT missense P193L variant present among multiple family members with autoimmune phenotypes led us to investigate whether TOP1MT could impact mtDNA mediated activation of the cGAS-STING innate immune response. We found

that the loss of TOP1MT in HCT116 cells led to increased levels of cytosolic mtDNA and activation of the cGAS-STING pathway, as reflected by increased levels of type I interferons. We confirmed the activation is explicitly through the cGAS activation using RU.521, which inhibits cGAS-mediated interferon upregulation without altering other inflammatory pathways[62]. We also investigated the impact of the P193L variant in the activation of this pathway. We found that low level re-expression of the P193L variant, close to endogenous levels, did not rescue the mtDNA release and cGAS-STING activation phenotype. However, ~10 fold overexpression of the P193L variant above endogenous protein expression was capable of fully reversing the cGAS-STING activation phenotype. These findings show that the P193L variant retains some functionality, which can provide rescue when overexpressed. However, at endogenous levels, the P193L variant was unable to reverse the cGAS-STING innate immune response in KO-ctrl cells, supporting the notion that this variant contributed to the autoimmune phenotypes in our family of interest.

In addition to the inability of the P193L variant to reverse cGAS-STING activation in cells lacking TOP1MT, we found that it was unable to rescue several other mitochondrial phenotypes linked to TOP1MT function (summarized in Table 2). Specifically, the P193L variant was only capable of partially rescuing nucleoid size, transcript levels, and mtDNA copy number recovery, despite high levels of expression of the P193L TOP1MT protein variant in HCT KO cells. Defects in these mtDNA related phenotypes are likely to be at least in part an indication of disrupted topoisomerase activity. Similarly, mitochondrial morphology was also only partially rescued by expression of the P193L variant. Although the mechanistic connection between TOP1MT and mitochondrial morphology remains unknown, it is tempting to speculate that this likely also involves the mtDNA.

The fact that the P193L variant was overexpressed by ~10 fold in our cellular model system, likely means that we are overestimating the partial functionality of this variant. Nonetheless, the P193L variant was unable to restore steady state levels of the OxPhos proteins, as well as several parameters of mitochondrial respiration, despite high levels of the re-expression. This finding suggests that the role of TOP1MT in mitochondrial translation, which is distinct from its topoisomerase activity, likely contributes to the reported mitochondrial dysfunction in patient blood cells. The finding that translation is more severely impaired than

topoisomerase activity for the P193L variant is similar to previous work for the two other TOP1MT variants[38].

P193L variant is located within the core barrel of TOP1MT, which is predicted to bind nucleic acids. Nonetheless, how the P193L variant mechanistically leads to cytosolic release of mtDNA remains unknown. Although *TOP1MT* is not yet formally characterized as a disease gene, increasing evidence suggests that some *TOP1MT* variants may indeed be pathogenic[38, 72, 73]. For example, an *in vitro* study showed that some TOP1MT variants have reduced DNA relaxation activities, including E168G, which has been described in a patient with mitochondrial deficiency syndrome[74]. Meanwhile, two other TOP1MT variants were identified in a patient with a pediatric cardiomyopathy[38]. The fact that the P193L variant we describe here segregated with autoimmune disease and SLE, suggests that this is a novel pathogenic phenotype linked to TOP1MT dysfunction. However, there are only a limited number of reports of potential pathogenic TOP1MT variants, which are associated with diverse pathogenic phenotypes. As such, more examples with shared phenotypes need to be identified before TOP1MT can officially be definitively considered as a disease gene. Nonetheless, future studies looking to establish the genetic cause of SLE should also consider variants in TOP1MT.

Genetic, epigenetic or environmental risk factors have been implicated as underlying causes of SLE[75]; however, the underlying mechanism behind the disease is not always clear. With respect to whether the P193L variant contributes to the SLE phenotype in our patient, it is important to consider some of the links between SLE and mitochondrial dysfunction. For example, general mitochondrial dysfunction and aberrant oxygen metabolism have a role in many autoimmune diseases, including SLE[76-78]. Meanwhile, links between SLE and the cGAS-STING innate immune response are also important in the context of considering the contribution of TOP1MT dysfunction to SLE. Consistent with the notion the cGAS-STING activation contributes to SLE, previous reports have noted cGAS-STING activation in a subset of SLE cases[79, 80]. Some of this previous work implicated nuclear DNA as the cytosolic dsDNA trigger, as studies identified impaired function of the nuclear DNA repair machinery can lead to SLE[81-87]. However, it is worth mentioning that much of the mitochondrial DNA repair machinery is shared with the nuclear repair machinery. Thus, it is likely that the impairments in nuclear DNA repair enzymes that are linked to SLE also impact mtDNA. The fact that some SLE patients exhibited increased levels of mtDNA damage[88] supports this notion and argues that

mtDNA damage may contribute to SLE. Moreover, it is notable that topoisomerases, including TOP1MT, can participate in DNA repair[89, 90]. Collectively, this previous work linking SLE, mitochondrial dysfunction, and the cGAS-STING pathway, support the argument that the P193L variant in TOP1MT contributes to SLE.

Another intriguing connection between SLE and TOP1MT is that fact that autoantibodies recognizing the nuclear topoisomerase enzyme TOP1 have been described in patients with SLE[43-46]. Notably, these TOP1 autoantibodies recognize the highly conserved catalytic domain of TOP1[91], which is conserved with TOP1MT. Given the novel connection that we describe here between TOP1MT and SLE, it is tempting to speculate that these autoantibodies are in fact made against TOP1MT and cross-react with TOP1, even though they were first shown to bind TOP1. This notion is supported by the fact that SLE sera recognize TOP1MT[92]. Given that 19% of autoantibodies collected from patients with SLE were able to detect TOP1MT[47], it is possible that TOP1MT plays a much wider role in SLE than currently appreciated. For example, if TOP1MT released from mitochondria along with mtDNA, these autoantibodies could also contribute to an elevated immune response contributing to SLE. Thus, beyond our current study, there is considerable evidence supporting the argument that TOP1MT plays a role in SLE.

The novel connection we describe here between TOP1MT, cGAS-STING and SLE has important therapeutic implications, as understanding the genetic basis of SLE, and identifying novel SLE candidate genes such as TOP1MT will be important for personalized medicine approaches. As we learn more about the different causes of SLE and their underlying mechanisms, this will provide a clearer picture of which treatments might be beneficial. For example, cGAS inhibitors like RU.521 may prove to be effective in patients where the cGAS-STING pathway is elevated. Additionally, it is important to consider the effects of drugs that impact TOP1MT function. A key example of a drug that impairs TOP1MT function is doxorubicin, which is a topoisomerase inhibitor used as low-dose chemotherapeutic[59, 74, 93]. Notably, doxorubicin causes mtDNA damage, cytosolic release of mtDNA, and activation of the cGAS-STING pathway[93]. While cGAS-STING activation by TOP1MT inhibitors may be advantageous by activating innate immune signaling in cancer[94], it could be detrimental in other circumstances by activating the immune response inappropriately.

Conclusions

In summary, this report provides the first evidence linking TOP1MT to release of mtDNA to the cytosol, activation of the innate immune response through the cGAS-STING pathway, and ultimately increased levels of interferons. These findings strongly support the notion that the P193L variant is responsible for the SLE phenotype in the patients and provide novel mechanistic insight how mitochondrial dysfunction can contribute to SLE via mtDNA-mediated activation of innate immunity. A better understanding of the causes of SLE will help to elucidate the complex heterogeneity of the disease, and lead to novel therapeutic approaches.

Funding: This work was supported by funds provided by the Alberta Children's Hospital Research Institute (ACHRI), the Alberta Children's Hospital Foundation (ACHF) and the Natural Sciences and Engineering Research Council of Canada (NSERC - RGPIN-2016-04083) (T.S.). This work was also supported by the NIH Intramural Program, the Center for Cancer Research, US National Cancer Institute (BC006161 to Y.P., H.Z and S.H.). W.T.G. was supported by a British Columbia Children's Hospital Institute (BCCHR) Intramural Investigator Grant Award Program (IGAP) award, and by a catalyst grant from Lupus Canada. I.A.K. is a recipient of an ACHRI Graduate Studentship and William H. Davies scholarship. A.K. received research funding from MitoCanada. The funding sources were not involved in the study design, data collection and analysis, the writing of the report, nor in the decision to submit.

Conflict of interest statement. The authors declare that they have no conflict of interest.

Author contributions: I.A.K. conceived the study, designed, performed, and analyzed experiments and wrote the manuscript. J.D. performed southwestern blot and cytosolic mtDNA experiments. S.S. generated the structural model. H.Z., S.H. and Y.P. generated the HCT116 *TOP1MT* KO cells, shared the TOP1MT cDNA, and provided input on the project. A.K. provided input on the project and edited the manuscript. W.T.G. identified the family bearing the *TOP1MT* patient variants, including clinical and family history, provided input on the project, and edited the manuscript. T.S. conceived and designed the study, analyzed experiments, supervised the study, and wrote the manuscript.

References

1. Wincup, C. and A. Radziszewska, *Abnormal Mitochondrial Physiology in the Pathogenesis of Systemic Lupus Erythematosus.* Rheum Dis Clin North Am, 2021. **47**(3): p. 427-439.
2. Yang, S.K., et al., *The Role of Mitochondria in Systemic Lupus Erythematosus: A Glimpse of Various Pathogenetic Mechanisms.* Curr Med Chem, 2020. **27**(20): p. 3346-3361.
3. Alperin, J.M., L. Ortiz-Fernández, and A.H. Sawalha, *Monogenic Lupus: A Developing Paradigm of Disease.* Front Immunol, 2018. **9**: p. 2496.
4. Bursztejn, A.C., et al., *Unusual cutaneous features associated with a heterozygous gain-of-function mutation in IFIH1: overlap between Aicardi-Goutières and Singleton-Merten syndromes.* Br J Dermatol, 2015. **173**(6): p. 1505-13.
5. An, J., et al., *Tartrate-Resistant Acid Phosphatase Deficiency in the Predisposition to Systemic Lupus Erythematosus.* Arthritis Rheumatol, 2017. **69**(1): p. 131-142.
6. Crow, Y.J., et al., *Characterization of human disease phenotypes associated with mutations in TREX1, RNASEH2A, RNASEH2B, RNASEH2C, SAMHD1, ADAR, and IFIH1.* Am J Med Genet A, 2015. **167a**(2): p. 296-312.
7. Dyall, S.D., M.T. Brown, and P.J. Johnson, *Ancient invasions: from endosymbionts to organelles.* Science, 2004. **304**(5668): p. 253-7.
8. Kukat, C., et al., *Super-resolution microscopy reveals that mammalian mitochondrial nucleoids have a uniform size and frequently contain a single copy of mtDNA.* Proc Natl Acad Sci U S A, 2011. **108**(33): p. 13534-9.
9. Kausar, S., et al., *Mitochondrial DNA: A Key Regulator of Anti-Microbial Innate Immunity.* Genes (Basel), 2020. **11**(1).
10. Cheng, Z., et al., *The Central Role and Possible Mechanisms of Bacterial DNAs in Sepsis Development.* Mediators Inflamm, 2020. **2020**: p. 7418342.
11. Luna-Sánchez, M., P. Bianchi, and A. Quintana, *Mitochondria-Induced Immune Response as a Trigger for Neurodegeneration: A Pathogen from Within.* Int J Mol Sci, 2021. **22**(16).
12. Riley, J.S. and S.W. Tait, *Mitochondrial DNA in inflammation and immunity.* EMBO Rep, 2020. **21**(4): p. e49799.
13. Lepelley, A., T. Wai, and Y.J. Crow, *Mitochondrial Nucleic Acid as a Driver of Pathogenic Type I Interferon Induction in Mendelian Disease.* Front Immunol, 2021. **12**: p. 729763.
14. Patrushev, M., et al., *Mitochondrial permeability transition triggers the release of mtDNA fragments.* Cell Mol Life Sci, 2004. **61**(24): p. 3100-3.
15. Kim, J., et al., *VDAC oligomers form mitochondrial pores to release mtDNA fragments and promote lupus-like disease.* Science, 2019. **366**(6472): p. 1531-1536.
16. Fang, C., X. Wei, and Y. Wei, *Mitochondrial DNA in the regulation of innate immune responses.* Protein Cell, 2016. **7**(1): p. 11-6.
17. Guo, Y., et al., *Mitochondrial DNA drives noncanonical inflammation activation via cGAS-STING signaling pathway in retinal microvascular endothelial cells.* Cell Commun Signal, 2020. **18**(1): p. 172.

18. Huang, L.S., et al., *mtDNA Activates cGAS Signaling and Suppresses the YAP-Mediated Endothelial Cell Proliferation Program to Promote Inflammatory Injury.* Immunity, 2020. **52**(3): p. 475-486.e5.
19. Bai, J., et al., *Mitochondrial stress-activated cGAS-STING pathway inhibits thermogenic program and contributes to overnutrition-induced obesity in mice.* Commun Biol, 2020. **3**(1): p. 257.
20. Decout, A., et al., *The cGAS-STING pathway as a therapeutic target in inflammatory diseases.* Nat Rev Immunol, 2021. **21**(9): p. 548-569.
21. Dobbs, N., et al., *STING Activation by Translocation from the ER Is Associated with Infection and Autoinflammatory Disease.* Cell Host Microbe, 2015. **18**(2): p. 157-68.
22. West, A.P., et al., *Mitochondrial DNA stress primes the antiviral innate immune response.* Nature, 2015. **520**(7548): p. 553-7.
23. Torres-Odio, S., et al., *Loss of Mitochondrial Protease CLPP Activates Type I IFN Responses through the Mitochondrial DNA-cGAS-STING Signaling Axis.* J Immunol, 2021. **206**(8): p. 1890-1900.
24. Matsui, H., et al., *Cytosolic dsDNA of mitochondrial origin induces cytotoxicity and neurodegeneration in cellular and zebrafish models of Parkinson's disease.* Nat Commun, 2021. **12**(1): p. 3101.
25. Sliter, D.A., et al., *Parkin and PINK1 mitigate STING-induced inflammation.* Nature, 2018. **561**(7722): p. 258-262.
26. Du, S., et al., *DNA sensing and associated type 1 interferon signaling contributes to progression of radiation-induced liver injury.* Cell Mol Immunol, 2021. **18**(7): p. 1718-1728.
27. Luo, X., et al., *Expression of STING Is Increased in Liver Tissues From Patients With NAFLD and Promotes Macrophage-Mediated Hepatic Inflammation and Fibrosis in Mice.* Gastroenterology, 2018. **155**(6): p. 1971-1984.e4.
28. Thomsen, M.K., et al., *The cGAS-STING pathway is a therapeutic target in a preclinical model of hepatocellular carcinoma.* Oncogene, 2020. **39**(8): p. 1652-1664.
29. Maekawa, H., et al., *Mitochondrial Damage Causes Inflammation via cGAS-STING Signaling in Acute Kidney Injury.* Cell Rep, 2019. **29**(5): p. 1261-1273.e6.
30. Chung, K.W., et al., *Mitochondrial Damage and Activation of the STING Pathway Lead to Renal Inflammation and Fibrosis.* Cell Metab, 2019. **30**(4): p. 784-799.e5.
31. Zhao, Q., et al., *STING Signaling Promotes Inflammation in Experimental Acute Pancreatitis.* Gastroenterology, 2018. **154**(6): p. 1822-1835.e2.
32. Sobek, S. and F. Boege, *DNA topoisomerases in mtDNA maintenance and ageing.* Exp Gerontol, 2014. **56**: p. 135-41.
33. Zhang, H., et al., *Human mitochondrial topoisomerase I.* Proc Natl Acad Sci U S A, 2001. **98**(19): p. 10608-13.
34. Zhang, X., et al., *Redox-induced apoptosis of human oocytes in resting follicles in vitro.* J Soc Gynecol Investig, 2006. **13**(6): p. 451-8.
35. Zhang, H. and Y. Pommier, *Mitochondrial topoisomerase I sites in the regulatory D-loop region of mitochondrial DNA.* Biochemistry, 2008. **47**(43): p. 11196-203.
36. Zhang, H., et al., *Increased negative supercoiling of mtDNA in TOP1mt knockout mice and presence of topoisomerases IIα and IIβ in vertebrate mitochondria.* Nucleic Acids Res, 2014. **42**(11): p. 7259-67.

37. Sobek, S., et al., *Negative regulation of mitochondrial transcription by mitochondrial topoisomerase I.* Nucleic Acids Res, 2013. **41**(21): p. 9848-57.
38. Khatib, I.A., et al., *Functional characterization of two variants in the mitochondrial topoisomerase gene TOP1MT that impact regulation of the mitochondrial genome.* bioRxiv, 2021: p. 2021.08.02.454711.
39. Han, S., et al., *Mechanisms of autoantibody production in systemic lupus erythematosus.* Front Immunol, 2015. **6**: p. 228.
40. Yaniv, G., et al., *A volcanic explosion of autoantibodies in systemic lupus erythematosus: a diversity of 180 different antibodies found in SLE patients.* Autoimmun Rev, 2015. **14**(1): p. 75-9.
41. Rekvig, O.P., *Anti-dsDNA antibodies as a classification criterion and a diagnostic marker for systemic lupus erythematosus: critical remarks.* Clin Exp Immunol, 2015. **179**(1): p. 5-10.
42. Bai, Y., et al., *Self-dsDNA in the pathogenesis of systemic lupus erythematosus.* Clin Exp Immunol, 2018. **191**(1): p. 1-10.
43. Fredi, M., et al., *Anti-topoisomerase-I antibodies in systemic lupus erythematosus and potential association with the presence of anti-dsDNA antibodies.* Lupus, 2017. **26**(10): p. 1121-1122.
44. Stojanov, L., et al., *Autoantibodies to topoisomerase I in a patient with systemic lupus erythematosus without features of scleroderma.* Lupus, 1995. **4**(4): p. 314-7.
45. Hamidou, M.A., et al., *Anti-topoisomerase I antibodies in systemic lupus erythematosus as a marker of severe nephritis.* Clin Rheumatol, 2006. **25**(4): p. 542-3.
46. Mahler, M., et al., *Anti-Scl-70 (topo-I) antibodies in SLE: Myth or reality?* Autoimmun Rev, 2010. **9**(11): p. 756-60.
47. Budde, P., et al., *Multiparametric detection of autoantibodies in systemic lupus erythematosus.* Lupus, 2016. **25**(8): p. 812-22.
48. Thim-Uam, A., et al., *STING Mediates Lupus via the Activation of Conventional Dendritic Cell Maturation and Plasmacytoid Dendritic Cell Differentiation.* iScience, 2020. **23**(9): p. 101530.
49. Li, Y., H.L. Wilson, and E. Kiss-Toth, *Regulating STING in health and disease.* J Inflamm (Lond), 2017. **14**: p. 11.
50. Jeremiah, N., et al., *Inherited STING-activating mutation underlies a familial inflammatory syndrome with lupus-like manifestations.* J Clin Invest, 2014. **124**(12): p. 5516-20.
51. Arneth, B., *Systemic Lupus Erythematosus and DNA Degradation and Elimination Defects.* Front Immunol, 2019. **10**: p. 1697.
52. Sabouny, R., et al., *Characterization of the C584R variant in the mtDNA depletion syndrome gene FBXL4, reveals a novel role for FBXL4 as a regulator of mitochondrial fusion.* Biochim Biophys Acta Mol Basis Dis, 2019. **1865**(11): p. 165536.
53. Donkervoort, S., et al., *MSTO1 mutations cause mtDNA depletion, manifesting as muscular dystrophy with cerebellar involvement.* Acta Neuropathol, 2019. **138**(6): p. 1013-1031.
54. Eaton, J.S., et al., *Ataxia-telangiectasia mutated kinase regulates ribonucleotide reductase and mitochondrial homeostasis.* J Clin Invest, 2007. **117**(9): p. 2723-34.
55. Khiati, S., et al., *Lack of mitochondrial topoisomerase I (TOP1mt) impairs liver regeneration.* Proc Natl Acad Sci U S A, 2015. **112**(36): p. 11282-7.

56. Baek, M., et al., *Accurate prediction of protein structures and interactions using a three-track neural network.* Science, 2021. **373**(6557): p. 871-876.
57. van Zundert, G.C.P., et al., *The HADDOCK2.2 Web Server: User-Friendly Integrative Modeling of Biomolecular Complexes.* J Mol Biol, 2016. **428**(4): p. 720-725.
58. Honorato, R.V., et al., *Structural Biology in the Clouds: The WeNMR-EOSC Ecosystem.* Front Mol Biosci, 2021. **8**: p. 729513.
59. Dalla Rosa, I., et al., *Mapping topoisomerase sites in mitochondrial DNA with a poisonous mitochondrial topoisomerase I (Top1mt).* J Biol Chem, 2014. **289**(26): p. 18595-602.
60. Baker, N.A., et al., *Electrostatics of nanosystems: application to microtubules and the ribosome.* Proc Natl Acad Sci U S A, 2001. **98**(18): p. 10037-41.
61. Gibson, W.T., et al., *Congenital leptin deficiency due to homozygosity for the Delta133G mutation: report of another case and evaluation of response to four years of leptin therapy.* J Clin Endocrinol Metab, 2004. **89**(10): p. 4821-6.
62. Vincent, J., et al., *Small molecule inhibition of cGAS reduces interferon expression in primary macrophages from autoimmune mice.* Nat Commun, 2017. **8**(1): p. 750.
63. Zhang, H., et al., *Increased negative supercoiling of mtDNA in TOP1mt knockout mice and presence of topoisomerases IIalpha and IIbeta in vertebrate mitochondria.* Nucleic Acids Res, 2014. **42**(11): p. 7259-67.
64. Yaginuma, K., et al., *A new RNA polymerase and in vitro transcription of the origin of replication from rat mitochondrial DNA.* Nucleic Acids Res, 1982. **10**(23): p. 7531-42.
65. Buzan, J.M. and R.L. Low, *Preference of human mitochondrial RNA polymerase for superhelical templates with mitochondrial promoters.* Biochem Biophys Res Commun, 1988. **152**(1): p. 22-9.
66. Fukuoh, A., et al., *DNA conformation-dependent activities of human mitochondrial RNA polymerase.* Genes Cells, 2009. **14**(8): p. 1029-42.
67. Barat-Gueride, M., C. Dufresne, and D. Rickwood, *Effect of DNA conformation on the transcription of mitochondrial DNA.* Eur J Biochem, 1989. **183**(2): p. 297-302.
68. Zollo, O. and N. Sondheimer, *Topological requirements of the mitochondrial heavy-strand promoters.* Transcription, 2017. **8**(5): p. 307-312.
69. Tang, J.X., et al., *Mitochondrial OXPHOS Biogenesis: Co-Regulation of Protein Synthesis, Import, and Assembly Pathways.* Int J Mol Sci, 2020. **21**(11).
70. Baechler, S.A., et al., *The mitochondrial type IB topoisomerase drives mitochondrial translation and carcinogenesis.* Nat Commun, 2019. **10**(1): p. 83.
71. Taguchi, T., et al., *STING Operation at the ER/Golgi Interface.* Front Immunol, 2021. **12**: p. 646304.
72. Wang, W., et al., *Identification of rare DNA variants in mitochondrial disorders with improved array-based sequencing.* Nucleic Acids Res, 2011. **39**(1): p. 44-58.
73. Khiati, S., et al., *Mitochondrial topoisomerase I (top1mt) is a novel limiting factor of doxorubicin cardiotoxicity.* Clin Cancer Res, 2014. **20**(18): p. 4873-81.
74. Zhang, H., et al., *Distribution bias and biochemical characterization of TOP1MT single nucleotide variants.* Sci Rep, 2017. **7**(1): p. 8614.
75. Kamen, D.L., *Environmental influences on systemic lupus erythematosus expression.* Rheum Dis Clin North Am, 2014. **40**(3): p. 401-12, vii.
76. Perl, A., *Pathogenic mechanisms in systemic lupus erythematosus.* Autoimmunity, 2010. **43**(1): p. 1-6.

77. Lood, C., et al., *Neutrophil extracellular traps enriched in oxidized mitochondrial DNA are interferogenic and contribute to lupus-like disease.* Nat Med, 2016. **22**(2): p. 146-53.
78. Leishangthem, B.D., A. Sharma, and A. Bhatnagar, *Role of altered mitochondria functions in the pathogenesis of systemic lupus erythematosus.* Lupus, 2016. **25**(3): p. 272-81.
79. An, J., et al., *Expression of Cyclic GMP-AMP Synthase in Patients With Systemic Lupus Erythematosus.* Arthritis Rheumatol, 2017. **69**(4): p. 800-807.
80. Kato, Y., et al., *Apoptosis-derived membrane vesicles drive the cGAS-STING pathway and enhance type I IFN production in systemic lupus erythematosus.* Ann Rheum Dis, 2018. **77**(10): p. 1507-1515.
81. Meas, R., M.J. Burak, and J.B. Sweasy, *DNA repair and systemic lupus erythematosus.* DNA Repair (Amst), 2017. **56**: p. 174-182.
82. Sallai, K., et al., *Antinucleosome antibodies and decreased deoxyribonuclease activity in sera of patients with systemic lupus erythematosus.* Clin Diagn Lab Immunol, 2005. **12**(1): p. 56-9.
83. Yasutomo, K., et al., *Mutation of DNASE1 in people with systemic lupus erythematosus.* Nat Genet, 2001. **28**(4): p. 313-4.
84. Al-Mayouf, S.M., et al., *Loss-of-function variant in DNASE1L3 causes a familial form of systemic lupus erythematosus.* Nat Genet, 2011. **43**(12): p. 1186-8.
85. Zervou, M.I., et al., *Association of the DNASE1L3 rs35677470 polymorphism with systemic lupus erythematosus, rheumatoid arthritis and systemic sclerosis: Structural biological insights.* Mol Med Rep, 2020. **22**(6): p. 4492-4498.
86. Lee-Kirsch, M.A., et al., *Mutations in the gene encoding the 3'-5' DNA exonuclease TREX1 are associated with systemic lupus erythematosus.* Nat Genet, 2007. **39**(9): p. 1065-7.
87. Fye, J.M., et al., *Dominant mutation of the TREX1 exonuclease gene in lupus and Aicardi-Goutieres syndrome.* J Biol Chem, 2011. **286**(37): p. 32373-82.
88. López-López, L., et al., *Mitochondrial DNA damage is associated with damage accrual and disease duration in patients with systemic lupus erythematosus.* Lupus, 2014. **23**(11): p. 1133-41.
89. Goffart, S., A. Hangas, and J.L.O. Pohjoismaki, *Twist and Turn-Topoisomerase Functions in Mitochondrial DNA Maintenance.* Int J Mol Sci, 2019. **20**(8).
90. Douarre, C., et al., *Mitochondrial topoisomerase I is critical for mitochondrial integrity and cellular energy metabolism.* PLoS One, 2012. **7**(7): p. e41094.
91. Piccinini, G., et al., *An antigenic region of topoisomerase I in DNA polymerase chain reaction-generated fragments recognized by autoantibodies of scleroderma patients.* Mol Immunol, 1991. **28**(4-5): p. 333-9.
92. Hongliang Zhang, M.K., and Yves Pommier, *Using mitochondrial TOP1 (TOP1mt) to probe the involvement of mitochondria in Systemic Lupus Erythematosus.*
93. Wu, Z., et al., *Mitochondrial DNA Stress Signalling Protects the Nuclear Genome.* Nat Metab, 2019. **1**(12): p. 1209-1218.
94. Jiang, M., et al., *cGAS-STING, an important pathway in cancer immunotherapy.* J Hematol Oncol, 2020. **13**(1): p. 81.

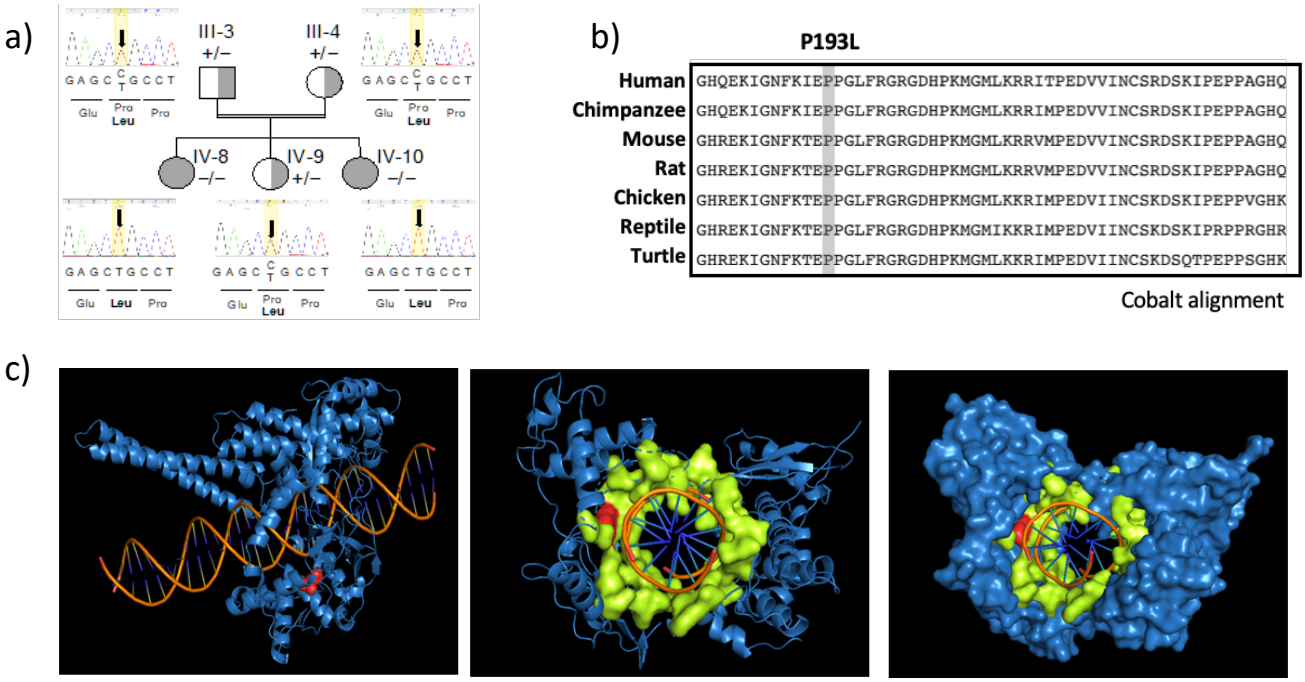

Figure 1. SLE Family with the P193L TOP1MT variant and protein structure. **a)** The pedigree structure of the affected family; the sequences show the nucleotide identity at position C578T where a missense Pro193Leu TOP1MT alteration was found. **b)** Amino acid alignments of TOP1MT proteins from a variety of vertebrate species generated using COBALT shows the conservation of the amino-acid variant identified in the affected family. **c)** c)Confirmation structure of TOP1MT showing the barrel for nucleic acid binding showing in Lime. Where the P193L mutation is shown in red.

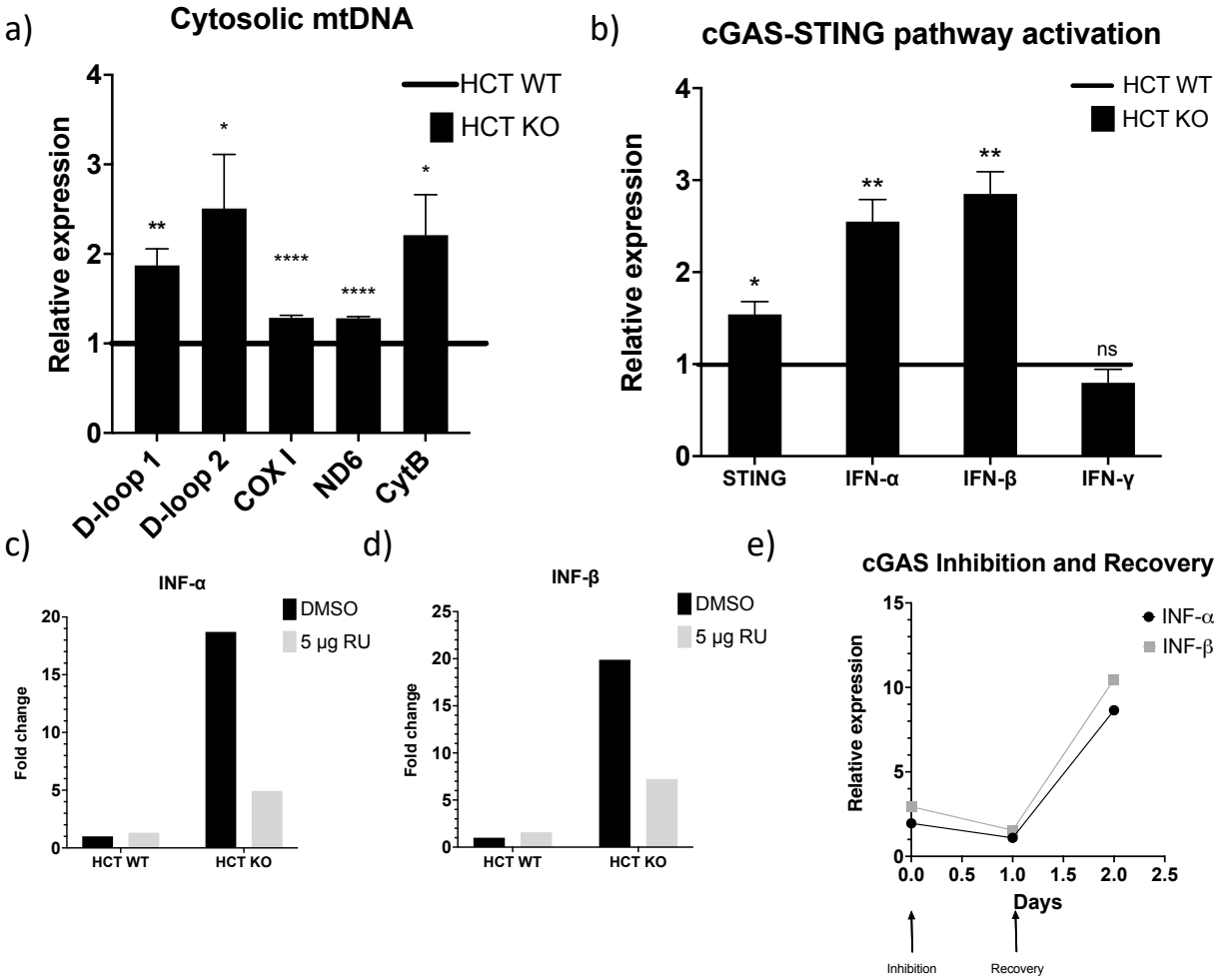

Figure 2. cGAS-STING pathway is activated in TOP1MT KO cells. **a)** Cytosolic mtDNA was quantitated via qPCR using the indicated primer sets and was found to be elevated in TOP1MT KO cells compared to WT cells. Normalization was done relative to the corresponding amplicons in total DNA. **b)** qRT-PCR analysis of STING, type I and type II interferons expression in TOP1MT KO cells compared to WT cells. **c,d)** cGAS inhibition by RU.521 lowers type I interferon expressions in TOP1MT-KO cells both INF- α (c) and INF-β (d) specifically in HCT KO cells. **e)** Recovery of TOP1MT KO cells in fresh media after cGAS inhibition by RU.521 show elevated interferon type I levels starting after 24 hrs of recovery. All statistical analysis were done using unpaired student t-test and p values * <0.05, ** <0.01 and **** <0.0001. 'ns' signifies no significant differences between indicated groups. Error bars represent standard error of mean.

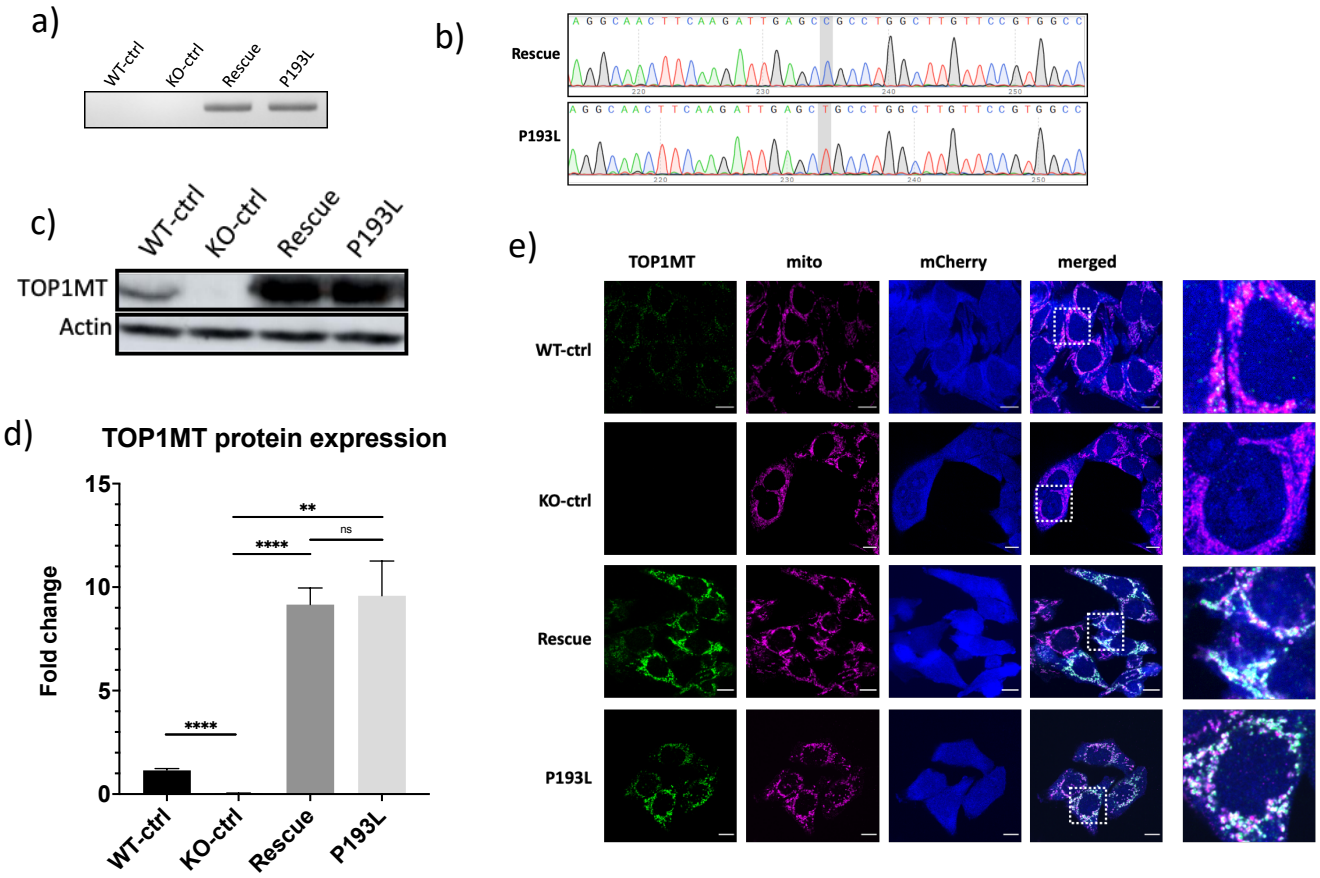

Figure 3. Generation of stable line expressing the variant form of TOP1MT. a) PCR amplification targeting the coding region of the viral-encoded *TOP1MT* open reading frame, spanning patient variant, confirms amplicons are present only in HCT-KO cell lines stably re-expressing *TOP1MT*, namely the Rescue and P193L lines. **b)** Chromatograms from Sanger sequencing of the amplicons produced from (c). The 578C residues (shaded), confirms the identity of the cell lines. **c)** Western blots probed for TOP1MT antibody confirms the TOP1MT expression in stably transduced cell lines. Actin was probed as a load control. **d)** Quantification of western blots from 4 replicates show the fold change in protein abundance compared to Actin control from four different replicates. All statistical analysis were done using unpaired student t-test; where error bars represent standard error of mean and p values ** <0.01, **** <0.0001 and 'ns' signifies no significant differences between indicated groups. Error bars represent standard error of mean. **e)** Representative confocal images of TOP1MT localization in stable lines where fixed Cells were stained for immunofluorescence with anti-TOMM20 (mitochondria, magenta) and anti-TOP1MT (green) primary antibodies. Viral transduction was confirmed by expression of mCherry (blue). The final column shows the zoomed-in region indicated in the merged column. Images confirm the mitochondrial localization of TOP1MT-P193L patient variant. Scale bar represent 10 µm.

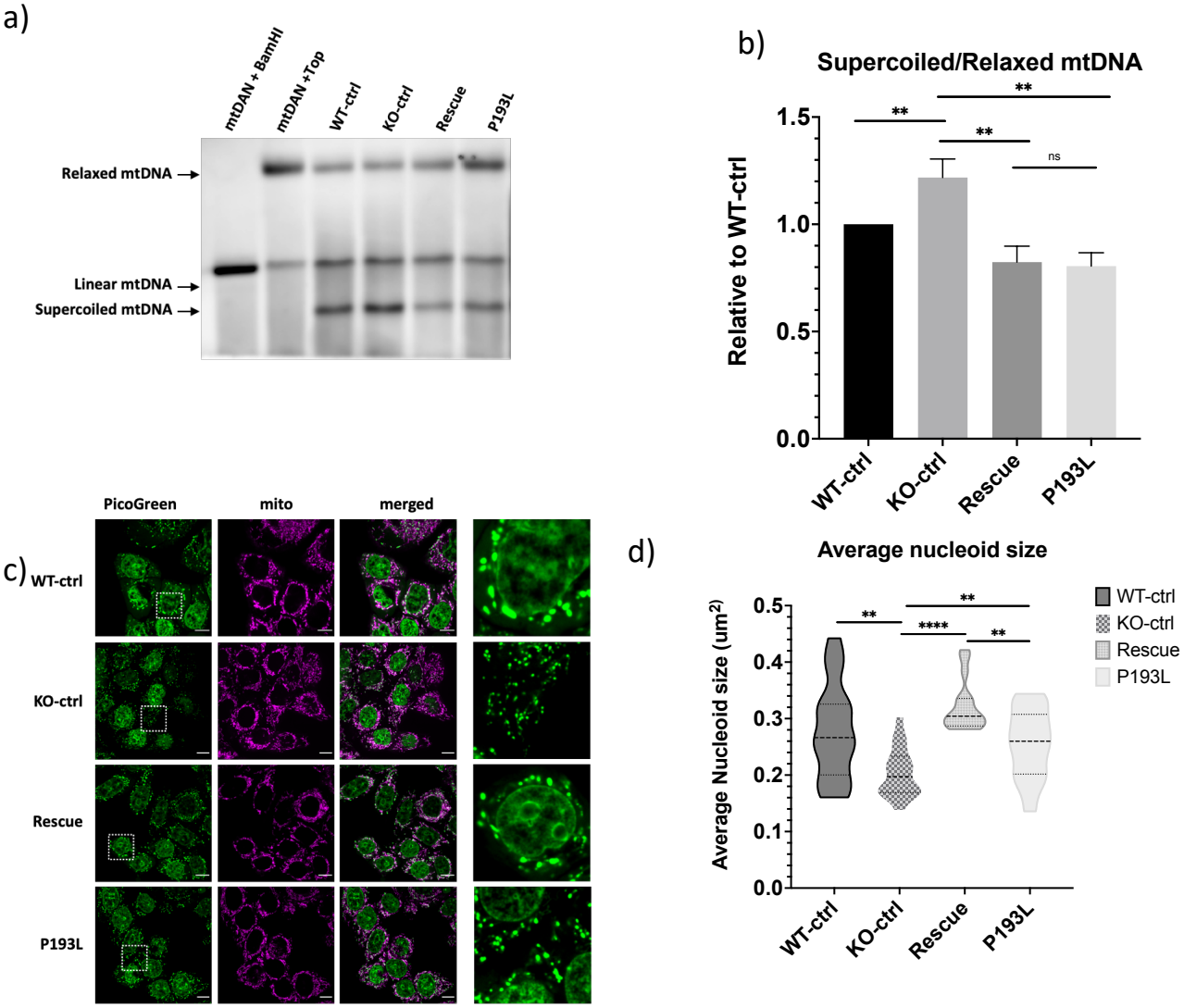

Figure 4. TOP1MT-KO cells stably expressing P193L alter mitochondrial genome supercoiling. **a)** Representative southwestern blots shows increased levels of the supercoiled mtDNA band in KO ctrl cells and P193L cells. **b)** Quantification of southwestern blots of different mtDNA forms as in (a), from four independent experiments, as a ratio of supercoiled to relaxed mtDNA. **c)** Representative confocal images of live cells stained with MitoTracker Far Red (mitochondria) and PicoGreen (dsDNA: nuclear and mtDNA) where the final column shows the zoomed-in of the dsDNA. Scalebars represent 10µm. Violin plots showing quantification of mtDNA nucleoids from 25 cells stained as in (c), represented as average nucleoid size per cell in **(d)**. All statistical analysis were done using unpaired student t-test and p values ** <0.01, **** <0.0001 and 'ns' signifies no significant differences between indicated groups. Error bars represent standard error of mean.

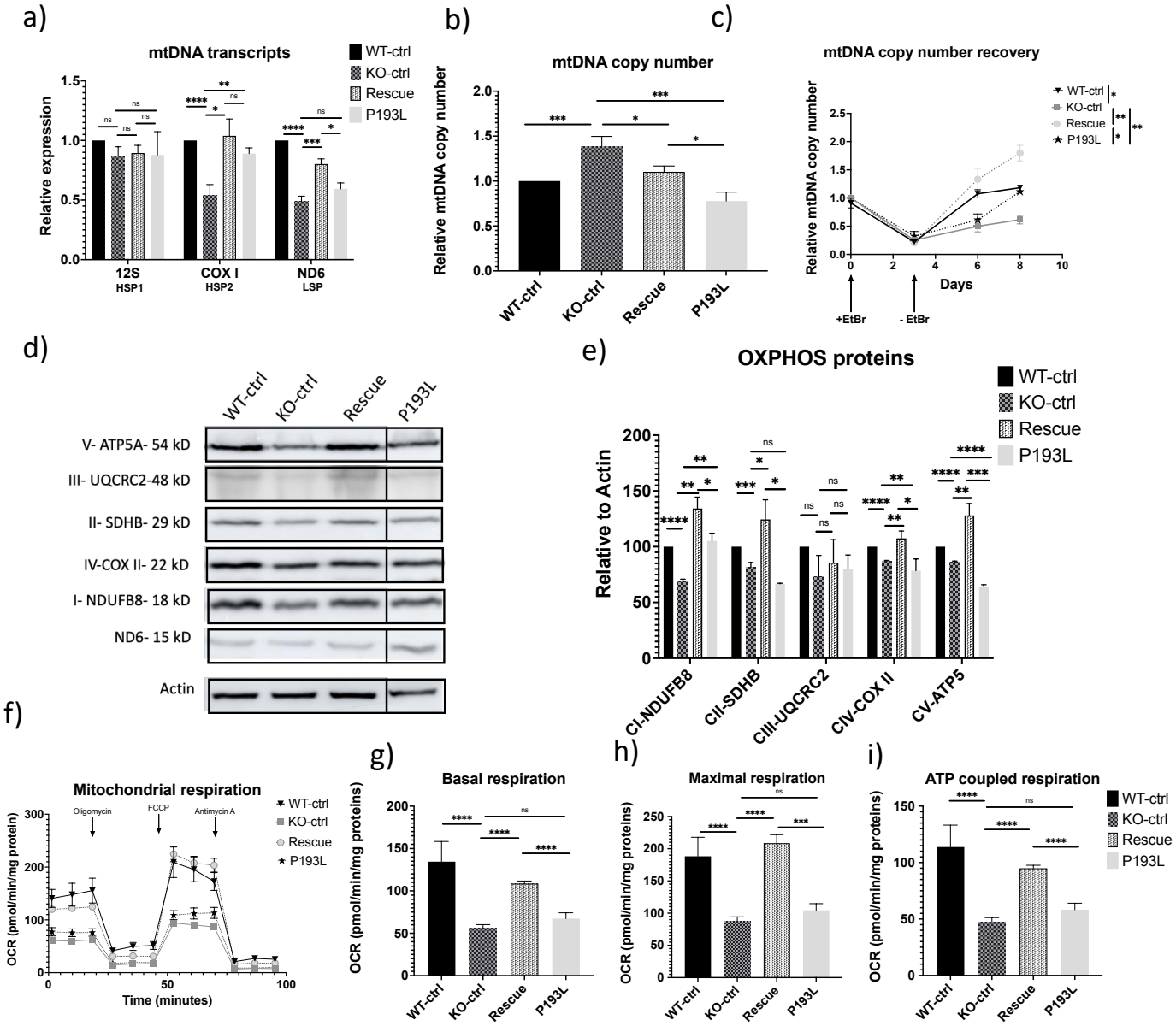

Figure 5. TOP1MT-KO cells stably expressing P193L affect mitochondrial DNA maintenance. **a)** Quantification of mtDNA transcripts in stable cell lines via quantitative RT-PCR for the indicated genes from the three mtDNA promoters: HSP1 (12S), HSP2 (COX I) and LSP (ND6) three independent biological replicates. **b)** Relative mtDNA copy number, determined by qPCR relative to 18S is rescued in P193L cells from three independent biological replicates. **c)** mtDNA copy number increases more slowly in P193L cells compared to Rescue cells following EtBr depletion for 3 days. **d)** Representative western blots show reduced levels of the indicated OXPHOS complex proteins in P193L cells Blots are cropped at the indicated sizes. **e)** Quantification of western blots of OXPHOS proteins as in (d), from three independent experiments, corrected to Actin as a load control. Reduction in OXPHOS proteins encoded by both nuclear (i.e. NDUFB8, SDHB, UQCRC2, ATP5) and mtDNA (i.e. COXII) genomes was observed in P193L cells lines. **f)** Oxygen consumption rates (OCR) over time analyzed in the indicated cell lines using the Seahorse XF24 extracellular flux analyzer. The OCR data was used to calculate basal respiration **(g)**, maximal respiration **(h)** and ATP production **(i)**. Data presented is from a representative experiment with 5 technical replicates. All statistical analysis were done using unpaired student t-test and p values * <0.05, ** <0.01, *** <0.001 and **** <0.0001. 'ns' signifies no significant differences between indicated groups. Error bars represent standard error of mean.

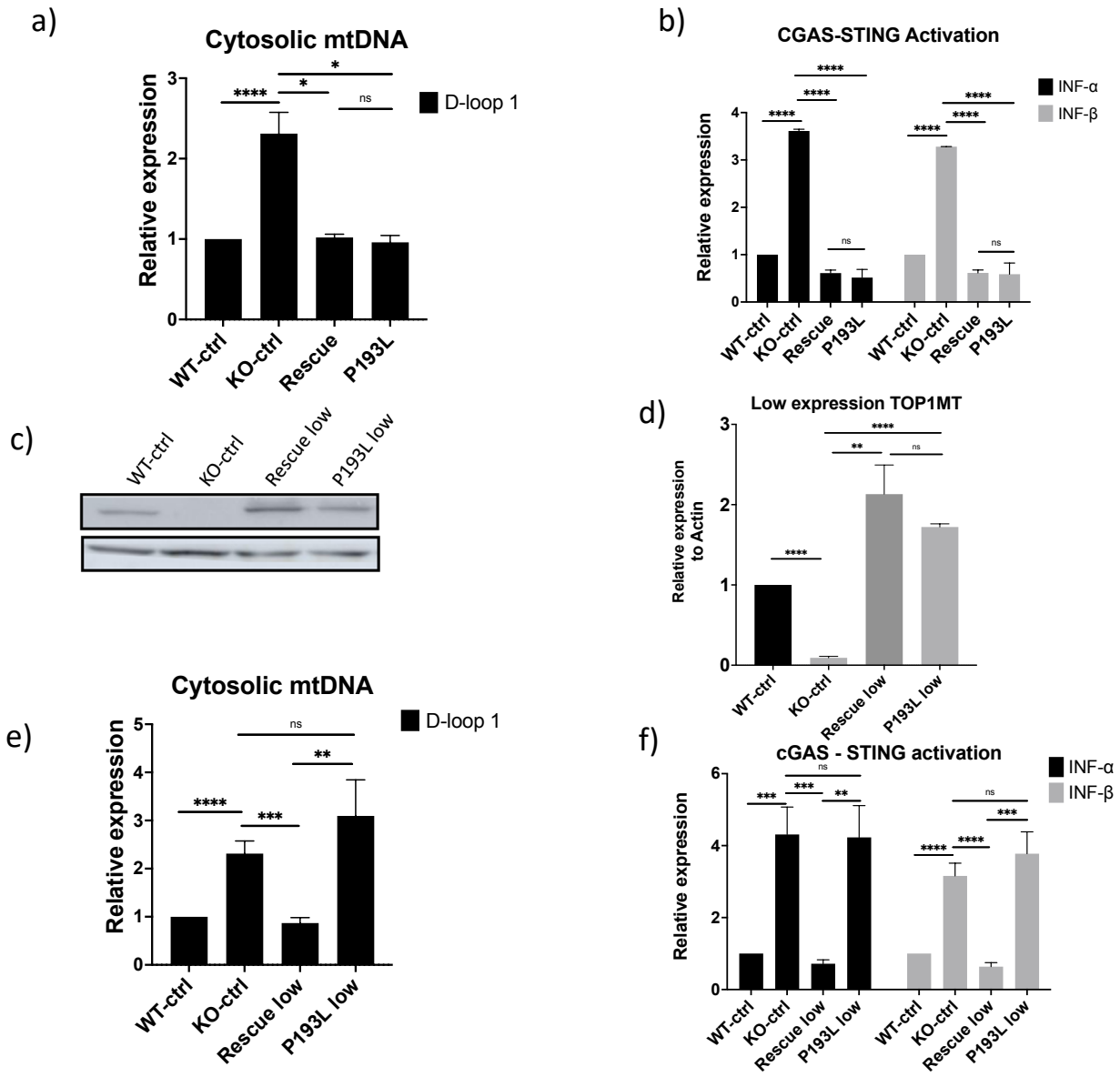

Figure 6. cGAS-STING pathway rescue in TOP1MT-KO cells stably expressing WT and P193L variants of TOP1MT. **a)** Cytosolic mtDNA levels were rescued by stably over expressing both WT and P193L forms of TOP1MT quantitated via qPCR using the indicated primer sets. Normalization was done relative to the corresponding amplicons in total DNA from the same cells. **b)** qRT-PCR analysis of type I interferon expression is rescued n TOP1MT KO cells over expression WT and P193L forms of TOP1MT.c**)** Representative western blots shows reduced levels of the TOP1MT protein in cells sorted for lower expression of both WT and P193L variants. **d)** Quantification of western blots of TOP1MT protein as in (c), from three independent experiments, corrected to Actin as a load control. **e)** Quantification of cytosolic mtDNA levels from cells as in (c) via qPCR using the indicated primer sets. Normalization was done relative to the corresponding amplicons in total DNA from the same cells. **f)** qRT-PCR analysis of type I interferon expression from cells as in (c) show elevated type I interferon levels in cells expressing moderate levels of P193L variant. All statistical analysis were done using unpaired student t-test and p values * <0.05, ** <0.01, *** <0.001 and **** <0.0001. 'ns' signifies no significant differences between indicated groups. Error bars represent standard error of mean.

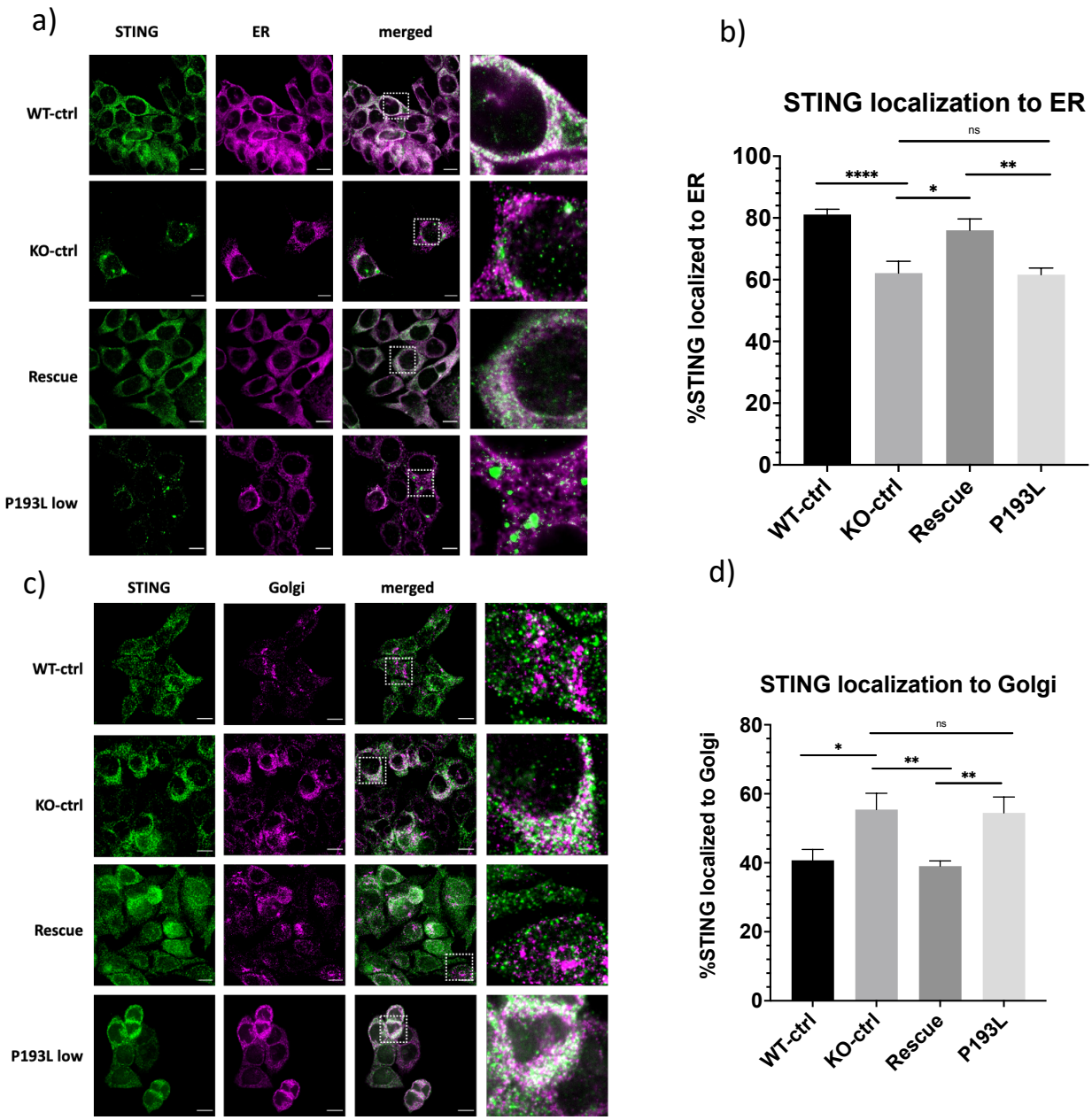

Figure 7. Activated STING relocates from the ER to the Golgi TOP1MT KO P193L cells. **a,c)** Representative confocal images of STING localization in stable lines with ER (a) and Golgi (c). Fixed Cells were stained for immunofluorescence with anti-STING (magenta) and anti-Calnexin (ER, magenta) or anti-TGN46 (Golgi, magenta) primary antibodies. The final column shows the zoomed-in region indicated in the merged column. Images confirm localization of STING to ER in TOP1MT WT and rescue cells and delocalisation to Golgi in TOP1MT KO as well as P193L cells. Scale bar represent 10 µm. **c,d)** Quantification of the percentage of STING localizing to the ER (b) or Golgi (d) from at least 10 images as in (a) and (c) respectively. All statistical analysis were done using unpaired student t-test and p values*<0.05, ** <0.01 and **** <0.0001. 'ns' signifies no significant differences between indicated groups. Error bars represent standard error of mean.

	KO-ctrl	Rescue	P193L
Nucleoid size	Smaller	+++	+
Supercoiling	Higher	+++	++
mtDNA Copy number	Higher	+++	+++
mtDNA Repletion	Slower	+++	++
Mitochondrial Transcripts	Lower	+++	+
OXPHOS Proteins	Lower	+++	+
Mitochondrial Oxygen consumption	Lower	+++	-
Mitochondrial morphology	Fused	+++	+
cGAS-STING activation	Activated	+++	++ High exp - Low exp

Table 2. Summary of analyzed phenotypes. Analyzed phenotypes where +++ represents full rescue, ++ represent moderate rescue, + for weak rescue and – for no rescue at all.